Heterogeneous Ultradense Networks With Traffic Hotspots: A Unified Handover Analysis

He Zhou, Haibo Zhou, *Senior Member, IEEE*, Jianguo Li, Kai Yang, *Member, IEEE*, Jianping An, *Senior Member, IEEE*, and Xuemin Shen, *Fellow, IEEE*

***Abstract*—With the ever-growing communication demands and the unceasing miniaturization of mobile devices, the Internet of Things is expanding the amount of mobile terminals to an enormous level. To deal with such numbers of communication data, plenty of base stations (BSs) need to be deployed. However, denser deployments of heterogeneous networks (HetNets) lead to more frequent handovers, which could increase network burden and degrade the users experience, especially in traffic hotspot areas. In this article, we develop a unified framework to investigate the handover performance of wireless networks with traffic hotspots. Using the stochastic geometry, we derive the theoretical expressions of average distances and handover metrics in HetNets, where the correlations between users and BSs in hotspots are captured. Specifically, the distributions of macro cells are modeled as independent Poisson point processes (PPPs), and the two tiers of small cells outside and inside the hotspots are modeled as PPP and Poisson cluster process (PCP) separately. A modified random waypoint (MRWP) model is also proposed to eliminate the density wave phenomenon in traditional models and to increase the accuracy of handover decision. By combining the PCP and MRWP model, the distributions of distances from a typical terminal to the BSs in different tiers are derived. Afterward, we derive the expressions of average distances from a typical terminal to different BSs and reveal that the handover rate, handover failure rate, and ping-pong rate are deduced as the functions of BS density, scattering variance of clustered small cell, user velocity, and threshold of triggered time. Simulation results verify the accuracy of the proposed analytical model and closed-form theoretical expressions.**

***Index Terms*—Handover analysis, heterogeneous networks (HetNets), Poisson cluster process (PCP), stochastic geometry.**

I. Introduction

DRIVEN by the development of Internet of Things (IoT), deploying the miniaturized terminals and dense base stations (BSs) in terrestrial communication networks is becoming the effective solution to meet the ever-growing demands of communication in hotspot areas [1], [2], [3], [4], [5]. In recent years, using stochastic geometry to model the spatial deployment of BSs in the IoT network has received significant attention from academics [6], [7]. In order to simulate the randomness of BSs distribution, the locations of BSs in different tiers are usually modeled as independent Poisson point processes (PPPs). Performing the signal-to-interference-plus-noise ratio (SINR) distribution analysis of multitier networks at a typical user, the coverage probability and outage probability are investigated in [8]. Although using PPP to model the random networks is tractable and convenient, it does not capture the coupling between BSs locations and user equipments (UEs) in hotspots, where the users and small BSs (SBSs) tend to be clustered. Since lots of achievements which focus on the PPP and further studies have been exhibited, we mainly pay our attention on the handover analysis based on the Poisson cluster processes (PCPs) where few studies are proposed in this area.

In this context, we consider using PCP, which has gained much attention on communication performance analysis in traffic hotspots to model the locations of BSs [9], [10]. Although the PCP-based model is suitable for characterizing ultradense networks, the innumerable diminutive mobile devices in the IoT network will bring complex handover management problems [11], [12], [13], [14]. As for the handover performance under the PCP-based model, Bao and Liang [15], [16] derived the analytical expressions for the rates of horizontal and vertical handoffs experienced by an active user with arbitrary movement trajectory. Specifically, Bao and Liang [15] considered using two tiers of PPP with different deployment intensities to model the locations of cluster centers and the cluster members. In the meantime, the set of $\triangle d$-extended is first introduced to quantify the 1-D measures of different length intensities on the 2-D plane. In [16], a stochastic geometric analysis framework on user mobility was proposed. The authors also provided guidelines for optimal tier selection under various user velocities, taking both the handoff rates and the data rate into consideration. However, the sojourn time for users which stay in the handover boundaries is not taken into consideration. To the authors' knowledge, only few

Manuscript received 13 January 2022; revised 7 May 2022 and 17 July 2022; accepted 23 December 2022. Date of publication 2 January 2023; date of current version 9 May 2023. This work was supported in part by the National Key Research and Development Program of China under Grant 2022YFC3301200, and in part by the National Natural Science Foundation of China under Grant 62201055. *(Corresponding authors: Jianguo Li; Kai Yang.)*

He Zhou and Kai Yang are with the School of Information and Electronics, Beijing Institute of Technology, Beijing 100811, China (e-mail: willzhou@bit.edu.cn; yangkbit@gmail.com).

Haibo Zhou is with the School of Electronic Science and Engineering, Nanjing University, Nanjing 210023, China (e-mail: haibozhou@nju.edu.cn).

Jianguo Li and Jianping An are with the School of Cyberspace Science and Technology, Beijing Institute of Technology, Beijing 100811, China (e-mail: jianguoli@bit.edu.cn; an@bit.edu.cn).

Xuemin Shen is with the Department of Electrical and Computer Engineering, University of Waterloo, Waterloo, ON N2L 3G1, Canada (e-mail: sshen@uwaterloo.ca).

Digital Object Identifier 10.1109/JIOT.2022.3233414

of the prior works focus on the handover analysis under PCP and take the sojourn time into consideration.

Recent developments in the field of stochastic geometry have led to a renewed interest with handover management in wireless networks [17], [18], [19], [20]. In stochastic geometry, the PPP is widely used in modeling and statistic analysis because of its universality and uniform distribution. Arshad et al. [21] proposed a cooperative handover management scheme to reduce unnecessary handovers in dense cellular networks. Furthermore, a velocity-aware mathematical model and an escalated handover scheme for the users were proposed in [22], in which the BSs along with the moving trajectory will be selected instead of those BSs which have stronger transmit power to maintain longer connection durations and to reduce handover rate. To quantify the performance of the proposed handover schemes via stochastic geometry, the effects of mobility on the densification gain were discussed in a two-tier downlink cellular network with ultradense small cells and C-plane/U-plane split architecture [23]. A joint bandwidth allocation and a call admission control strategy were proposed in [24] to reduce unnecessary handovers. The authors proposed joint optimization of cell association and power control that maximizes the long-term system-wide utility in [25] to reduce the handover rate. A joint optimization of cell association and power control solution was also proposed in [26] to improve the spectrum and energy efficiency and reduce the handover rate. For handover analysis, the closed-form theoretical expressions of handover rate, handover failure rate, and ping-pong rate were investigated in [27], where the distribution of BSs' locations follow independent PPP and the expressions were resolved as a function of BS density and triggered time threshold. With redefined definitions, the handover rate in this article decouples with the handover failure rate. Compared with [27], the handover rate is more specific and accurate since it only contains the influence of user mobility model and sojourn time inside the equal long-term biased DL-RSS boundary (ERB) circles. Moreover, according to the description in [28], the handover failure rate in this article is denoted as the number of handover failures divided by the handover triggered numbers.

Although PPP is tractable in modeling the deployment of BSs, it is not suitable enough to capture the coupling between UEs and BSs in traffic hotspots, thus motivating Saha et al. [10], [29] to model the BSs and users in ultradense area using PCPs. The performance of coverage probability for a typical device-to-device (D2D) receiver under two realistic scenarios was investigated in [30]. The analysis quantifies the best and worst performance of clustered D2D networks in terms of coverage probability and area spectral efficiency. In order to capture the correlation between clustered BSs and users in high-density area, the downlink coverage probability was discussed in cellular networks modeled by the Thomas cluster process (TCP) and Matérn cluster process in [31]. In [32], the performance of coverage probability and throughput was studied in heterogeneous networks (HetNets) under two association policies, the simulations demonstrated that with the increasing reusability of the same resource block for small cells, the coverage probability decreases whereas throughput increases.

Based on the former research, it is well accepted that using the random spatial point process to model the distribution of BSs is more realistic when compared with the traditional hexagonal model [33], [34] in ultradense networks. In the aforementioned papers, the distribution of SBSs is usually assumed to be the same as the macro BSs (MBSs) to reduce the analytical and computational complexity. But in the practical circumstances, especially in the urban area, the clustered SBSs or the users are usually nonhomogeneously distributed. For instance, in the city planning, several specific areas are chosen as the economic or educational centers. Those geographical centers usually have higher population density and communication demand compared with other areas [35]. And the movement trajectory of targets in those area tends to limit in a specific region. This phenomenon brings the edge effects into our study. In that case, the practical location of SBSs among those centers is the superposition of nonuniform distributions. In order to capture those features, we model the locations of SBSs clustered on the hotspots as PCP. Moreover, in order to get the convincing handover analysis results, the selection of the mobility model is quite important. It is essential to choose an appropriate mobility model to analyze how the movement of users affects the network performance. Normally, the researchers select the random waypoint (RWP) model because of its tractability in modeling movement patterns of mobile nodes [36]. Lin et al. [37] provided an improved traceable mobility model which shows better performance in emerging cellular networks when compared with the classical RWP mobility model and the synthetic truncated Levy walk model. However, the aforementioned RWP model has some inherit disadvantages, such as the nodes tend to concentrate on the center [38] and the transition length scales with the size of the area.

In this article, to overcome the difficulties that the traditional BSs deployment scheme cannot apply in the hotspots areas, we develop a PCP-based BSs deployment scheme to model the practical BSs distribution by considering the correlation between clustered BSs and users. Compared with [15] and [16], in our manuscript, we derive not only the handover rate but also the handover failure rate and ping-pong rate to further investigate the handover performance in hotspots area. Moreover, in our PCP-based model, the handover rate also consists of the probability that the sojourn time for each user inside the ERB is larger than the threshold. By considering the sojourn time of users inside the ERB circles, the prediction of the handover rate is more accurate and reliable. In our revised manuscript, the location of the target BS is not restricted to any direction or any tier. The corresponding coordinate of target BS can be random point in the entire simulation region. Moreover, the average distance between different BSs under TCP is also presented, which is first proposed recently, to solve the handover problems in hotspots. Note that the density wave phenomenon (DWP) indicates that the nodes distributed in a finite area tend to concentrate on the center under RWP model [27], [39], which will bring the edge effects into our analysis. In this case, users have less probability to intersect

with those BSs near the edge areas. Therefore, we propose a modified RWP (MRWP) model to overcome the DWP and to increase the accuracy of handover decision in the boundary region. Compared with the small cell coverage model in [27], where the target SBS is assumed in the horizontal direction of MBS, we adjust the coordinates of SBSs to ensure that the analysis of the small cell coverage model is suitable for any SBS in the coverage area. In that case, the analysis of the small cell coverage model is suitable for any SBS in the coverage area.

Incorporating the spatial coupling and the MRWP model, we first derive the closed-form expressions of handover rate, handover failure rate, and ping-pong rate. Then, extensive simulations are conducted to validate the theoretical results and to analyze how the user mobility affects the handover performance in hotspot areas.

The main contributions of this article are as follows.

1) Novel BSs deployment scheme and MRWP model are proposed. We develop a practical HetNets model for traffic hotspots area, where the locations of users and clustered SBSs are coupled in hotspots to capture the correlation. We also propose an MRWP model to eliminate the density wave phenomenon in hotspots area and to increase the accuracy of handover decision.
2) New distances distributions and average distances are derived. Considering the method proposed in [40] using a sum of finite exponential series to obtain the approximate expression of the integral of the first kind modified Bessel function, we derive the closed-form expressions of average distances from one SBS to other BSs, handover rate, handover failure rate, and ping-pong rate under TCP scenario.
3) The accuracy of the theoretical results is verified through simulations. The effects and the tradeoff of system parameters, such as BS density, the scattering variance of TCP, thresholds of triggered time, and user mobility on the handover performances, are studied to provide guidance for future network planning in ultradense HetNets.

TABLE I
NOTATIONS AND DESCRIPTIONS OF PARAMETERS

Parameters	Descriptions
$\lambda_{\mathrm{M}}, \lambda_{\mathrm{S}}, \lambda_{\mathrm{S}'}$	Densities of MBSs, PPP-SBSs, and PCP-SBSs.
$\Phi_{\mathrm{M}}, \Phi_{\mathrm{S}}, \Phi_{\mathrm{S}'}$	Locations of MBSs, PPP-SBSs, and PCP-SBSs.
λ_p, σ	Density of parent point and scattering standard variance of offspring point for $\Phi_{\mathrm{S}'}$.
P_i, G_i	Transmit power and antenna gain of BSs in the i-th tier.
C_i, α_i	Path-loss intercept and exponent in the i-th tier.
B_i	Association bias of the i-th tier.
L_k	Rayleigh distributed initial transition length in the k-th movement with parameter σ_{RWP}.
μ_k	Bernoulli distributed indicator of transition length extension in the k-th movement with parameter p_Z.
Z_k	Rayleigh distributed extended transition length in the k-th movement with parameter σ_Z.
V_k	User velocity during the k-th movement.
S_k	User pause time after the k-th movement.
R_{ij}	Distance from a random point inside Φ_i to the nearest point inside Φ_j, $i, j \in \{\mathrm{M}, \mathrm{S}, \mathrm{S}'\}$.
$\bar{R}_{ij}$	Average distance from a random point inside Φ_i to the nearest point inside Φ_j, $i, j \in \{\mathrm{M}, \mathrm{S}, \mathrm{S}'\}$.
$H_{\mathrm{t},ij}$	Handover triggered rate from tier i to tier j.
H_{ij}	Handover rate from tier i to tier j.
$H_{\mathrm{f},ij}$	Handover failure rate from tier i to tier j.
$H_{\mathrm{p},ij}$	Ping-pong rate from tier i to tier j.
T	Time threshold of handover failure event.
T_p	Time threshold of Ping-pong event.

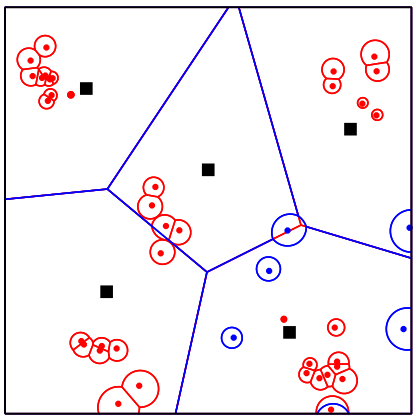

Fig. 1. Illustrations of the BSs deployment model. The black square represents the location of MBS. The blue dot and the blue circle around it represent the location of SBS following PPP and its ERB, respectively. The red dot and the red circle around it represent the location of SBS following TCP and its ERB, respectively.

II. System Model

A. BS Deployment Model

We consider a three-tier HetNet consisting of uniformly deployed MBSs and SBSs in general area and clustered SBSs in hotspot area, as shown in Fig. 1. The macro cells mainly provide global coverage and support the necessary signaling transmission [27], while the small cells are allocated with specific frequency to provide local area coverage and basic communication services. Specifically, the locations of uniform MBSs and SBS are assumed to follow homogeneous PPPs Φ_M and Φ_S in the plane with density λ_M and λ_S, respectively. Regarding the clustered SBSs, inspired by the fact that SBSs in the hotspot areas are usually geographically clustered, to capture the spatial correlation, we model these SBSs as a TCP $\Phi_{S'}$ generated from a parent point process Φ_p. Here, Φ_p is a homogeneous PPP with density λ_p, and the SBSs are independently and identically scattered around the cluster centers of Φ_p following a symmetric normal distribution with variance σ^2. Therefore, the probability density function (PDF) of distance R from the offspring point to the cluster center can be expressed as

$$f_R(r) = \frac{1}{2\pi\sigma^2} \exp\left(-\frac{r^2}{2\sigma^2}\right), \quad r \geq 0. \tag{1}$$

Thus, $\Phi_{S'}$ can be equivalently expressed as $\Phi_{S'} = \bigcup_{z\in\Phi_p} B_z$, where B_z is the subset of $\Phi_{S'}$ generated from the parent point $z \in \Phi_p$.

B. User Mobility Model

Based on the improved RWP model in [27], the user's kth movement can be represented by $(\boldsymbol{X}_{k-1}, \boldsymbol{X}_k, V_k, S_k)$, where $\boldsymbol{X}_{k-1}$ is the starting waypoint, $\boldsymbol{X}_k$ is the target waypoint, V_k is the velocity, and S_k is the pause time of user staying at $\boldsymbol{X}_k$. Given the starting waypoint $\boldsymbol{X}_{k-1}$, the transition length $L_k = \|\boldsymbol{X}_k - \boldsymbol{X}_{k-1}\|$ follows a Rayleigh distribution with parameter σ_{RWP} and the direction is uniformly distributed in $[0, 2\pi]$. By adjusting σ_{RWP}, the average transition can be changed to model the movement patterns of users in infinite region. According to [38], the DWP will affect the accuracy of handover probability calculation. It can be ignored when the simulation area is sufficiently large, in which the number of points near the edge are small. However, as we described in Section I, the trajectories of users in hotspots are usually clustered in finite regions. Thus, the improved RWP model proposed in [27], which is designed for infinite planes, will not be suitable for our limited finite regions. In our manuscript, the handover analysis is conducted on a hotspot area, and the edge effect will thus bring difficulties to our handover performance analysis. To minimize the impact of DWP, we propose the MRWP model by inducing a Rayleigh distributed extra distance Z to extend the trajectory of each movement with a certain chance while keeping the direction unchanged. Specifically, the transition length after extension in MRWP is formulated by

$$L'_k = L_k + \mu_k Z_k \tag{2}$$

where μ_k is a Bernoulli random variable with parameter p_Z and Z_k is a Rayleigh random variable with PDF given by

$$f_{Z_k}(z) = \frac{z}{\sigma_Z^2} \exp\left(-\frac{z^2}{2\sigma_Z^2}\right), \quad z \geq 0. \tag{3}$$

Z_k is the extra distance in the user's kth movement. And μ_k represents the probability of extending the original movement trajectory L_k with the extra distance Z_k. The PDF of Z_k follows the Rayleigh distribution since the original movement L_k follows the Rayleigh distribution. Besides, we assume that the velocity V_k and the pause time S_k are independently and identically distributed with PDF $f_V(\cdot)$ and $f_S(\cdot)$, respectively.

To validate the effectiveness of the MRWP model, we separate the simulation region into five subregions in Fig. 2(a). The occurrence probabilities of users in these regions under the RWP model and MRWP model are presented in Fig. 2(b). Compared with the RWP model, the MRWP model results in higher occurrence probability in the boundary region and more uniform waypoints in the whole region, which shows that the handover analysis under the MRWP model is more reliable and convincing.

C. Channel Model and Association Strategy

According to 3GPP standards, a handover procedure will be processed in four layers. We consider the method in [27] where prefect filtering is adopted in Layer-1 and Layer-4. Since the prefect filtering is deployed and dynamic resource allocation is assumed to average the fading and noise. Several related works also take similar assumptions in their analyses [27], [29]. The

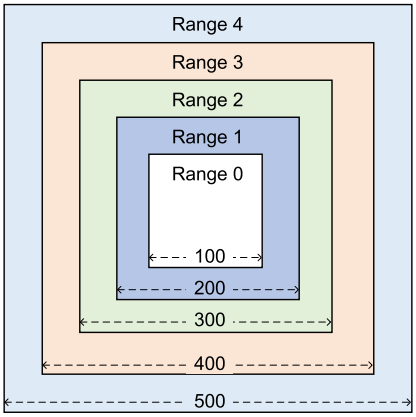

(a)

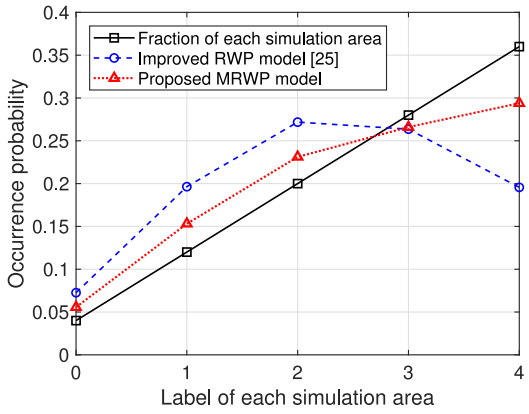

(b)

Fig. 2. Partition of simulation area and the occurrence probability for MRWP model and improved RWP model. (a) Illustration of separated simulation areas. (b) Occurrence probability.

link experiences power-law path loss. The handover procedure usually takes the instantaneous reference signal received power (RSRP) as the indicator to initiate or terminate the process. We assume that the BSs in the ith tier have identical transmit power P_i and antenna gain G_i, $i \in \{M, S, S'\}$. The RSRP can be simplified to the downlink received signal strength (DL-RSS) as

$$\text{RSS}_i(r) = B_i P_i G_i C_i r^{-\alpha_i} \tag{4}$$

where r is the distance from the typical terminal to the BS in tier i, B_i represents the association bias which aims at adjusting the coverage range of BS to achieve load balance, C_i is the path loss at reference distance, and α_i is the path-loss exponent. Along the mobility trajectory, the user will choose the BS which provides the strongest DL-RSS as the next serving BS. The handover boundary for each BS is then determined by the ERB [41].

III. Handover Boundary and Distance Distribution Analysis

In this section, we first determine the approximate expressions of handover boundary and handover failure boundary, and then derive the distribution of the distance between the BSs that the user is served by before and after handover. These

metrics will be used to characterize the handover performance in traffic hotspot area in Section IV.

A. Handover Boundary Analysis

Consider a typical BS $X_i \in \Phi_i$ at origin and a target BS $X_j \in \Phi_j$, the ERB $\mathscr{B}_{X_iX_j}$ is composed of the points at which the DL-RSSs received from X_i and X_j are identical, i.e.,

$$\mathscr{B}_{X_iX_j} = \left\{X \in \mathbb{R}^2 \mid \mathrm{RSS}_i(d_i) = \mathrm{RSS}_j(d_j)\right\} \tag{5}$$

where $d_i = \|X - X_i\|$ and $d_j = \|X - X_j\|$. Recalling (4) and the Cartesian coordinates $X_i = (0,0)$, $X_j = (x_j, y_j)$, $X = (x, y)$, the condition in (5) can be rewritten as

$$\xi_{ij}\left(x^2 + y^2\right)^{\alpha_{ij}} - \left[\left(x - x_j\right)^2 + \left(y - y_j\right)^2\right] = 0 \tag{6}$$

where $\xi_{ij} = (B_jP_jG_jC_j/(B_iP_iG_iC_i))^{2/\alpha_j}$ and $\alpha_{ij} = \alpha_i/\alpha_j$ [42]. For analytical tractability, we approximate $f(x,y) = (x^2+y^2)^{\alpha_{ij}}$ with $\tilde{f}(x,y) = \lambda(x^2+y^2)$ by minimizing $E_\lambda(x,y)$, where

$$\begin{aligned} E_\lambda(x,y) &= \left|f(x,y) - \hat{f}(x,y)\right| \\ &= \left|\left(x^2+y^2\right)^{\alpha_{ij}} - \lambda\left(x^2+y^2\right)\right|. \end{aligned} \tag{7}$$

Converting coordinates from Cartesian to polar, we can rewrite $E_\lambda(x,y)$ to

$$E_\lambda(r) = \left|r^{2\alpha_{ij}} - \lambda r^2\right| \tag{8}$$

where $r = \sqrt{x^2+y^2}$. The optimal λ can then be expressed as

$$\lambda^* = \arg\min_{\lambda} \int_0^{\sqrt{x_j^2+y_j^2}} E_\lambda(r)dr. \tag{9}$$

The exact expression of λ^* is given in the following lemma.

Lemma 1: λ^* is determined by $\lambda^* = (x_j^2 + y_j^2)^{\alpha_{ij}-1}$.

Proof: See Appendix A. ∎

Then, leveraging Lemma 1 and substituting $f(x,y)$ with $\tilde{f}(x,y|\lambda^*)$, the ERB in (5) can be approximated by a circle $\mathcal{B}(\tilde{X}, \tilde{R})$, where the center $\tilde{X}$ and radius $\tilde{R}$ are, respectively, given by

$$\tilde{X} = \left(\frac{x_j}{1-\lambda^*\xi_{ij}}, \frac{y_j}{1-\lambda^*\xi_{ij}}\right), \tilde{R} = \frac{\sqrt{\lambda^*\xi_{ij}\left(x_j^2+y_j^2\right)}}{1-\lambda^*\xi_{ij}}. \tag{10}$$

The approximated closed-form circular equation of the handover initial process is presented in (10). Similarly, the handover failure boundary can be approximated by $\mathcal{B}(\tilde{X}_f, \tilde{R}_f)$ with

$$\tilde{X}_f = \left(\frac{x_j}{1-\lambda^*\xi_{f,ij}}, \frac{y_j}{1-\lambda^*\xi_{f,ij}}\right), \tilde{R}_f = \frac{\sqrt{\lambda^*\xi_{f,ij}\left(x_j^2+y_j^2\right)}}{1-\lambda^*\xi_{f,ij}} \tag{11}$$

where $\xi_{f,ij} = \xi_{ij}Q_{\mathrm{out}}^{2/\alpha_j}$ and $Q_{\mathrm{out}} < 1$. Once the UE moves into the handover triggered circle, the threshold time T starts. If the UE steps into the handover failure circle within T, the handover process failed. Based on the aforementioned analysis, the ERB functions of handover and handover failure are approximated by the circular equations as shown in Fig. 3. Combining the MRWP model and handover boundary analysis, the handover rate and handover failure rate can be determined by the number of UEs' trajectory intersecting with $\mathcal{B}(\tilde{X}, \tilde{R})$ and $\mathcal{B}(\tilde{X}_f, \tilde{R}_f)$ in the unit time, respectively.

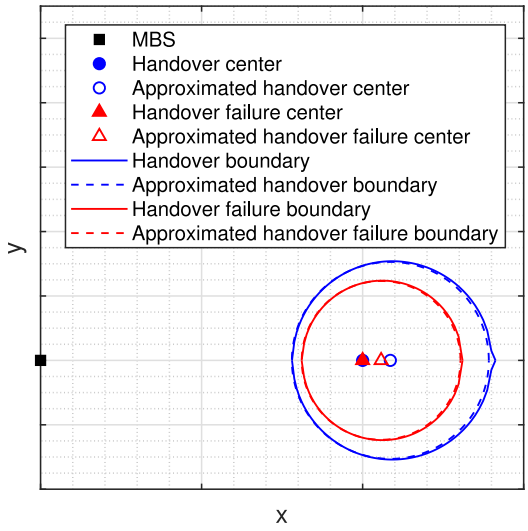

Fig. 3. Approximate solution of handover circle boundary and handover failure circle boundary.

B. Handover Strategy

In this article, by combining the MRWP model and BSs deployment under prefect filtering and dynamic resource allocation, the users can switch between different BSs according to DL-RSS. The handover process is divided into two subprocesses, termed as handover triggered process and the sojourn time process. The handover event, handover failure event, and the ping-pong event are defined as follows.

1) Only if the user crosses the boundary of handover circle and stays inside handover ERB longer than T, a handover procedure is determined as successful.
2) As for the handover failure process, when the user crosses the boundary of handover failure circle, in the meantime, the sojourn time between handover ERB and handover failure ERB is smaller than T, The handover procedure is determined as unsuccessful.
3) For the ping-pong process, after the handover procedure is initiated, the typical user returns to the original BS service area before the sojourn time is greater than T_p inside the target cell. In that case, a ping-pong procedure is determined as successful.

To be noted that each of the above handover events, including the handover event, handover failure event, and the ping-pong event, occurs on the premise of handover triggered event occurring.

C. Distance Distribution

For the analysis of the average distances and handover performance in the proposed model, we need to get the distribution of those relevant distances from the two kinds of SBSs to the MBS. Let R_{ij} denote the distances from $x_i \in \Phi_i$ to the nearest BS in Φ_j. Since the coverage area is a circle according to Section III-A, we approximate R_{ij} by its average value. $R_{S'M}$ represents the distance from a typical SBS in $\Phi_{S'}$ to the nearest MBS in Φ_M. R_{SM} represents the distance from

a typical SBS in Φ_S to the nearest MBS in Φ_M. As for $R_{S'S}$, which represents the distance from a typical SBS in $\Phi_{S'}$ to the nearest SBS in Φ_S.

1) R_{SM}: The PDF and CDF of R_{SM} are given by

$$f_{R_{\mathrm{SM}}}(r) = 2\pi\lambda_m r \exp\left(-\pi\lambda_m r^2\right) \tag{12}$$

$$F_{R_{\mathrm{SM}}}(r) = 1 - \exp\left(-\pi\lambda_m r^2\right) \tag{13}$$

respectively.

2) $R_{S'S}$: Assuming the typical BS located at the origin, the distribution of $R_{S'S}$ conditioned on the hotspot center location is given in the following theorem.

Theorem 1: Conditioned on the distance from the hotspot center to the origin being W_S, the conditional PDF and CDF of $R_{S'S}$ are

$$f_{R_{S'S}|W_S}(r|w) = \frac{r}{\sigma^2}\exp\left(-\frac{r^2+w^2}{2\sigma^2}\right)I_0\left(\frac{wr}{\sigma^2}\right) \tag{14}$$

$$F_{R_{S'S}|W_S}(r|w) = 1 - Q_1\left(\frac{w}{\sigma^2}, \frac{r}{\sigma^2}\right) \tag{15}$$

respectively, where $f_{W_S}(w) = 2\pi\lambda_S w\exp(-\pi\lambda_S w^2)$, I_0 is the modified Bessel function of the first kind, and $Q_1(\cdot)$ is the Marcum Q-function.

Proof: See Appendix B. ∎

3) $R_{S'M}$: As for $R_{S'M}$, which represents the distance from a typical SBS in $\Phi_{S'}$ to the nearest MBS in Φ_M. Similar to $R_{S'S}$, the conditional PDF and CDF of $R_{S'M}$ can be expressed as

$$f_{R_{S'M}|W_M}(r|w) = \frac{r}{\sigma^2}\exp\left(-\frac{r^2+w^2}{2\sigma^2}\right)I_0\left(\frac{wr}{\sigma^2}\right) \tag{16}$$

$$F_{R_{S'M}|W_M}(r|w) = 1 - Q_1\left(\frac{w}{\sigma^2}, \frac{r}{\sigma^2}\right) \tag{17}$$

where $f_{W_M}(w) = 2\pi\lambda_M w\exp(-\pi\lambda_M w^2)$.

D. Mean Distance

The handover rate can be separated into the handover triggered rate and the probability that the mobile terminal's sojourn time inside the target cell is larger than the threshold. To obtain the handover triggered rate under different distances distributions, it is essential to calculate the average values of R_{SM}, $R_{S'S}$, and $R_{S'M}$.

1) $\bar{R}_{\mathrm{SM}}$: The average value of R_{SM} can be obtained by

$$\bar{R}_{\mathrm{SM}} = \mathbb{E}[R_{\mathrm{SM}}] = \int_0^\infty r f_{R_{\mathrm{SM}}}(r)\,dr = \frac{1}{2\sqrt{\lambda_M}}. \tag{18}$$

2) $\bar{R}_{S'S}$: The average value of $R_{S'S}$ can be expressed as

$$\bar{R}_{S'S} = \mathbb{E}[R_{S'S}] = \mathbb{E}_{W_S}\left[\int_0^\infty r f_{R_{S'S}|W_S}(r)dr\right]. \tag{19}$$

Substituting (14) into (19) yields

$$\bar{R}_{S'S} = \int_0^\infty\int_0^\infty \frac{2\pi\lambda_S w r^2}{\sigma^2}\exp\left(-\frac{r^2+w^2}{2\sigma^2} - \pi\lambda_S w^2\right) \times I_0\left(\frac{wr}{\sigma^2}\right)drdw. \tag{20}$$

To obtain the closed-form expression of $\bar{R}_{S'S}$, we approximate $I_0(z)$ by the sum of a finite exponential series [40], i.e.,

$$I_0(z) \approx \sum_{k=1}^{4} a_k e^{b_k z} \tag{21}$$

TABLE II
VALUES OF a_k AND b_k IN (20) FOR DIFFERENT INTERVALS OF z

$0 \le z < 11.5$		$11.5 \le z < 20$		$20 \le z < 37.25$		$z \ge 37.25$	
a_k	b_k	a_k	b_k	a_k	b_k	a_k	b_k
0.1682	0.7536	0.2667	0.4710	0.1121	0.9807	$2.4e^{-9}$	1.144
0.1472	0.9736	0.4916	−163.4	0.1055	0.8672	0.0675	0.995
0.4450	−0.715	0.1110	0.9852	$-1.8e^{-4}$	1.0795	0.0547	0.567
0.2382	0.2343	0.1304	0.8554	0.0033	1.0385	0.0787	0.946

where a_k and b_k are presented in Table II. Therefore, substituting (21) into (20), $\bar{R}_{S'S}$ can be simplified to

$$\bar{R}_{S'S} = \sum_{k=1}^{4}\frac{2\pi\lambda_S a_k}{\sigma^2}\int_0^\infty w e^{-\left(\frac{1}{2\sigma^2}+\pi\lambda_S\right)w^2}F_k(w)dw \tag{22}$$

where

$$F_k(w) = \int_0^\infty r^2\exp\left(-\frac{r^2}{2\sigma^2} + \frac{b_k wr}{\sigma^2}\right)dr. \tag{23}$$

By invoking [43, eq. (3.462.7)], $F_k(w)$ can be evaluated by

$$F_k(w) = \sigma^2 b_k w + \sqrt{\frac{\pi}{2}}\left(\sigma b_k^2 w^2 + \sigma^3\right)e^{\frac{b_k^2 w^2}{2\sigma^2}} \times\left[1 + \mathrm{erf}\left(\frac{b_k w}{\sqrt{2}\sigma}\right)\right] \tag{24}$$

where $\mathrm{erf}(x) = (2/\sqrt{\pi})\int_0^x \exp(-y^2)dy$ is the error function.

Since $\mathrm{erf}(x) < 1$, $x \ge 0$, we obtain an upper bound of $F_k(w)$ as follows:

$$F_k^{(ub)}(w) = \sqrt{2\pi}\left(\sigma b_k^2 w^2 + \sigma^3\right)e^{\frac{b_k^2 w^2}{2\sigma^2}} + \sigma^2 b_k w. \tag{25}$$

Substituting $F_k^{(ub)}(w)$ into (22), we obtain an upper bound of $\bar{R}_{S'S}$ as follows:

$$\begin{aligned}\bar{R}_{S'S}^{(ub)} &= \sum_{k=1}^{4}\frac{2\pi\lambda_S a_k}{\sigma^2}\int_0^\infty \sigma^2 b_k w^2 e^{-\left(\pi\lambda_S+\frac{1}{2\sigma^2}\right)w^2} \\ &\quad + \sqrt{2\pi}w\left(\sigma b_k^2 w^2 + \sigma^3\right)e^{-\left(\pi\lambda_S+\frac{1-b_k^2}{2\sigma^2}\right)w^2}dw \\ &= \sum_{k=1}^{4}\sqrt{2\pi}q_S\sigma a_k\left[\frac{2}{(2q_S+1-b_k^2)}\right. \\ &\quad \left. + \frac{b_k}{(2q_S+1)^{3/2}} + \frac{4b_k^2}{(2q_S+1-b_k^2)^2}\right]\end{aligned} \tag{26}$$

where $q_S = \pi\lambda_S\sigma^2$.

3) $\bar{R}_{S'M}$: Similarly, the average value of $\bar{R}_{S'M}$ is upper bounded by

$$\begin{aligned}\bar{R}_{S'M}^{(ub)} &= \sqrt{2\pi}q_M\sigma\sum_{k=1}^{4}a_k\left[\frac{2}{(2q_M+1-b_k^2)}\right. \\ &\quad \left. + \frac{b_k}{(2q_M+1)^{3/2}} + \frac{4b_k^2}{(2q_M+1-b_k^2)^2}\right]\end{aligned} \tag{27}$$

where $q_M = \pi\lambda_M\sigma^2$.

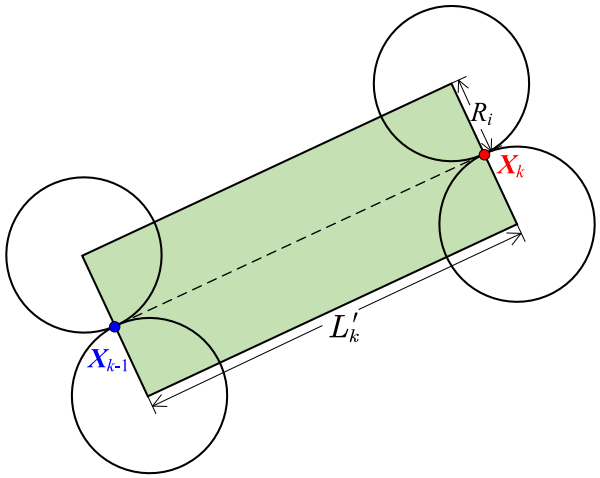

Fig. 4. Illustration of the region in which the BS intersects with users' trajectory.

IV. Handover Performance Analysis

In this section, we give the definitions of handover rate, handover failure rate, and ping-pong rate. By formulating different handover procedures into several subprocesses, the theoretical expressions of these handover metrics under different BS densities and scattering variances of TCP are obtained.

A. Handover Rate

According to the MRWP model, the trajectory of UE is divided into finite segments by setting the start waypoints and target waypoints. The handover triggered rate is defined as the number of crosspoints of each UE's trajectory intersecting with the ERB circle in the unit time. According to Section II-B, the length of each movement is determined by $L'_k = L_k + \mu_k Z_k$. During each movement, the handover event is triggered when the trajectory of the user intersects with the ERB circle, i.e., the distance from the nearest target BS to the trajectory of this movement is smaller than $\bar{R}_\ell$, $\ell \in \{\mathrm{SM}, S'M, S'S\}$. Since each trajectory and the radius of ERBs are finite, the BSs have to stay in the specific area to ensure that their ERBs can intersect with the user's trajectory. We approximate this specific area as a rectangle with length L'_k and width $\bar{R}_\ell$. As shown in Fig. 4, the length is user's trajectory and the width is the distance from the center of the nearest ERB circle $\mathcal{B}(\tilde{X}, \tilde{R})$ to the user's trajectory. Thus, the specific area for each target BS can be expressed as $2L'_k\bar{R}_\ell$. On the entire coverage, the probability that each target BS can be reached by user's trajectory is $(2L'_k\bar{R}_\ell/|\mathcal{S}|)$. Moreover, the corresponding radius of target BS may be smaller than the average distance $\bar{R}_\ell$, for those BSs located inside the area of $2L'_k\bar{R}_\ell$ with smaller average radius, the handover triggered event will not be initiated successfully. In order to solve this problem, we consider using the handover circle boundary intensity to describe the probability that the transition length L'_k intersects with the handover circle boundary during each movement [44]. Arshad et al. [44] considered the general expression of the handover rate from the kth tier to the jth tier as a function of $\mu(\tau_{kj})$, which represents the expected length of cell boundaries in a unit square. Since it is difficult to conduct the analysis on the cell boundaries, we extend the cell boundaries by an infinitesimal width Δd. Note that the probability of having the user on the Δd-extended cell boundary is equivalent to the expected area of the boundary in a unit square, which is expressed as the area intensity $\mu(\tau_{kj}^{(\Delta d)})$. Since the handover boundary is simplified as circle in Section III-A and the average number of target BSs in different tiers can be expressed as $\mathbb{E}[N_{\mathrm{BS},\ell}]$. The area intensity of different handover circles can be expressed as

$$\mu\left(\tau_\ell^{(\Delta d)}\right) = \frac{\mathbb{E}\left[N_{\mathrm{BS},\ell}\right] \cdot \left(\pi\left(\bar{R}_\ell + \Delta d\right)^2 - \pi\left(\bar{R}_\ell - \Delta d\right)^2\right)}{|\mathcal{S}|} \tag{28}$$

where $\ell \in \{\mathrm{SM}, S'M, S'S\}$. The average number of target BSs $\mathbb{E}[N_{\mathrm{BS},\ell}] = \lambda_\ell \mathcal{S}$, $\lambda_\ell \in \{\lambda_M, \lambda_M, \lambda_S\}$. Letting $\Delta d \to 0$, we can get the expression of handover circle length intensity $\mu(\tau_\ell)$ as

$$\begin{aligned}\mu(\tau_\ell) &= \lim_{\Delta d \to 0} \frac{\mu\left(\tau_\ell^{(\Delta d)}\right)}{2\Delta d} \\ &= \frac{\mathbb{E}\left[N_{\mathrm{BS},\ell}\right] 2\pi \bar{R}_\ell}{|\mathcal{S}|}\end{aligned} \tag{29}$$

where the average distance of $\bar{R}_\ell$ is obtained in (18), (26), and (27).

In Fig. 4, we can see that a handover is initiated if the handover boundary intersects with L'_k inside the $2L'_kR_\ell$ area. However, the handover events may not occur successfully because of the actual distance R_ℓ may smaller than $\bar{R}_\ell$. Thus, we calculate the handover rings boundaries in each $\mathcal{S}_k = 2L'_kR_\ell$ rather than the average specific area $\bar{\mathcal{S}}_k = 2L'_k\bar{R}_\ell$ as shown in Fig. 4.

For instance, the radius R_ℓ of handover circle $\mathcal{B}(\tilde{X}, \tilde{R})$ is quite small and the user's movement trajectory L'_k does not touch the boundary of $\mathcal{B}(\tilde{X}, \tilde{R})$. However, because the center of $\mathcal{B}(\tilde{X}, \tilde{R})$ locates inside $\bar{\mathcal{S}}_k = 2L'_k\bar{R}_\ell$, this handover is determined as success even L'_k does not touch the boundary of $\mathcal{B}(\tilde{X}, \tilde{R})$. Thus, the handover rate will be inaccurate since the handovers may be higher than the expected results. In order to solve this problem, we came up the idea of using handover circle length intensity to determine if the handover event is successfully triggered when the center of target BS locates inside $2L'_kR_\ell$. For each movement of users, the handover occurs in $\mathcal{S}_k$. The length of handover boundaries inside $\mathcal{S}_k$ can down to zero when the center of target BS locates on L'_k, or equal to πR_ℓ when L'_k is the tangent line of handover boundary circle of target BS. And the threshold M is constructed to determine if the sum of handover boundaries during this movement is greater enough to trigger the handover event. Which means the threshold M for area intensity $\tau_{L',\ell}$ is constrained by $0 < M \leq \pi R_\ell$. $\mathbb{P}(\tau_{L',\ell} \geq M)$ is present to analyze how the user mobility model influences the handover performance. It represents the probability of the area of handover boundary is greater than the predefined threshold M and it helps to get accurate handover triggered rate. Take the maximum value of threshold M as πR_ℓ, the probability that handover boundaries area $\tau_{L',\ell}$ during each movement is greater than the threshold M can be

expressed as

$$\mathbb{P}\left(\tau_{L',\ell} \geq M\right) = \mathbb{P}\left(\mu(\tau_\ell) \cdot 2L'_k R_\ell \geq \pi R_\ell\right) = \mathbb{P}\left(L'_k \geq \frac{1}{4\lambda_\ell \bar{R}_\ell}\right). \tag{30}$$

Note that L'_k is a mixed distribution function with $\mathbb{E}[L'_k] = (1/[2\sqrt{\sigma_{\text{RWP}}}]) + \mu_k\sqrt{(\pi/2)}\sigma_Z$. In order to get the expression of CDF of L'_k, we assume that the MRWP model follows a Rayleigh distribution with average value of $\mathbb{E}[L'_k] = (1/[2\sqrt{\sigma_{\text{MRWP}}}]) = (1/[2\sqrt{\sigma_{\text{RWP}}}]) + \mu_k\sqrt{(\pi/2)}\sigma_Z$. Thus, we can derive the expression of $\mathbb{P}(L'_k \geq [1/(4\lambda_\ell \bar{R}_\ell)])$ as

$$\mathbb{P}\left(L'_k \geq \frac{1}{4\lambda_\ell \bar{R}_\ell}\right) = \exp\left\{-\frac{\sigma_{\text{MRWP}}\pi}{\left(4\lambda_\ell \bar{R}_\ell\right)^2}\right\} = \exp\left\{\frac{-\pi}{\left(\frac{1}{\sigma_{\text{RWP}}} + \frac{2\mu_k\sqrt{2\pi}\sigma_Z}{\sqrt{\sigma_{\text{RWP}}}} + 2\pi\mu_k^2\sigma_Z^2\right)\cdot\left(4\lambda_\ell \bar{R}_\ell\right)^2}\right\} \tag{31}$$

where

$$\sigma_{\text{MRWP}} = \frac{1}{\left(\frac{1}{\sigma_{\text{RWP}}} + 2\mu_k\pi\frac{\sqrt{\sigma_Z}}{\sqrt{\sigma_{\text{RWP}}}} + \mu_k^2\pi^2\sigma_Z\right)}.$$

Thus, the expression of the handover triggered rate for one target BS can be expressed as

$$H_{t,\ell}^{(\text{single})} = \frac{1}{|\mathcal{S}|}\int_0^\infty\int_0^\infty 2lrf_{L_k}(l)f_{R_\ell}(r)dldr \cdot \mathbb{P}\left(L'_k \geq \frac{1}{4\lambda_\ell \bar{R}_\ell}\right) \tag{32}$$

where $\mathcal{S}$ is the entire area and $\ell \in \{\text{SM}, S'M, S'S\}$. Leveraging the independence between L_k and R_ℓ and substituting (10) into (32) yield

$$H_{t,\ell}^{(\text{single})} = \frac{2}{|\mathcal{S}|}\frac{\sqrt{\lambda^*\xi}}{1-\lambda^*\xi}\mathbb{E}\left[L'_k\right]\mathbb{E}[R_\ell] \cdot \mathbb{P}\left(L'_k \geq \frac{1}{4\lambda_\ell \bar{R}_\ell}\right) \tag{33}$$

which can be further simplified by using $\mathbb{E}[L'_k] = (1/[2\sqrt{\sigma_{\text{MRWP}}}])$. For convenience, we take the same assumption of $\mathbb{E}[S_k] = 0$ in [27] and [37]. We obtain the handover triggered rate as follows:

$$H_{t,\ell} = \frac{\mathbb{E}\left[N_{bs,\ell}\right]H_{t,\ell}^{(\text{single})}}{\frac{\mathbb{E}\left[L'_k\right]}{\mathbb{E}[V_k]} + \mathbb{E}[S_k]} = 2\frac{\sqrt{\lambda^*\xi}\lambda_\ell \bar{R}_\ell V}{1-\lambda^*\xi}\exp\left\{-\frac{\pi\sigma_{\text{MRWP}}}{\left(4\lambda_\ell \bar{R}_\ell\right)^2}\right\}. \tag{34}$$

It is notable that the handover procedure may not be eventually executed when it is successfully triggered. According to [27], the average sojourn time is formulated by

$$S_\ell = \frac{\pi R_\ell\sqrt{\lambda^*\xi}}{2V(1-\lambda^*\xi)}. \tag{35}$$

Then, the probability that the UE stays in the ERB circle longer than the threshold T is given by

$$\mathbb{P}(S_\ell \geq T) = \begin{cases} \exp\left(-\frac{4\lambda_M V^2T^2(1-\lambda^*\xi)^2}{\pi\lambda^*\xi}\right), & \ell = \text{SM} \\ Q_1\left(\frac{1}{2\sigma\sqrt{\lambda_S}}, \frac{2TV(1-\lambda^*\xi)}{\pi\sigma\sqrt{\lambda^*\xi}}\right), & \ell = S'S \\ Q_1\left(\frac{1}{2\sigma\sqrt{\lambda_M}}, \frac{2TV(1-\lambda^*\xi)}{\pi\sigma\sqrt{\lambda^*\xi}}\right), & \ell = S'M \end{cases} \tag{36}$$

respectively. Finally, as has been discussed in Section III-B, the handover rate is determined by

$$H_\ell = H_{t,\ell}\mathbb{P}(S_\ell \geq T). \tag{37}$$

B. Handover Failure Rate

The handover procedure is determined to be failed when the received SINR is smaller than Q_{out} or the sojourn time is smaller than T. The handover failure rate, which is identical to the handover failure numbers divided by the handover triggered numbers in a unit time, can be expressed as

$$H_{f,\ell} = \frac{H_{f,t,\ell}\mathbb{P}\left(S_{f,\ell} \leq T\right)}{H_{t,\ell}} \tag{38}$$

where $H_{f,t,\ell}$ is the handover failure triggered rate, and $S_{f,\ell}$ is the sojourn time for the typical UE between handover boundary and handover failure boundary. Similar to (34), $H_{f,t,\ell}$ can be expressed as

$$H_{f,t,\ell} = 2\frac{\sqrt{\lambda^*\xi_f}\lambda_\ell \bar{R}_\ell V}{1-\lambda^*\xi_f}\exp\left\{-\frac{\pi\sigma_{\text{MRWP}}}{\left(4\lambda_\ell \bar{R}_\ell\right)^2}\right\}. \tag{39}$$

And $\mathbb{P}(S_{f,\ell} \leq T)$ can be expressed as

$$\mathbb{P}\left(S_{f,\ell} \leq T\right) = \begin{cases} 1 - \exp\left(-\frac{4\lambda_M V^2T^2(1-\lambda^*\xi_f)^2}{\pi\lambda^*\xi_f}\right), & \ell = \text{SM} \\ 1 - Q_1\left(\frac{1}{2\sigma\sqrt{\lambda_S}}, \frac{2TV(1-\lambda^*\xi_f)}{\pi\sigma\sqrt{\lambda^*\xi_f}}\right), & \ell = S'S \\ 1 - Q_1\left(\frac{1}{2\sigma\sqrt{\lambda_M}}, \frac{2TV(1-\lambda^*\xi_f)}{\pi\sigma\sqrt{\lambda^*\xi_f}}\right), & \ell = S'M. \end{cases} \tag{40}$$

C. Ping-Pong Rate

The ping-pong rate, which can be defined as the probability that after the handover procedure is initiated, the typical user returns back to the original BS's serving region in the time period T_{p}. According to [27], the ping-pong rate $H_{\text{p},\ell}$ is formulated by

$$H_{\text{p},\ell} = H_{t,\ell}\left[\mathbb{P}\left(S_\ell \leq T_{\text{p}}\right) - \mathbb{P}(S_\ell \leq T)\right]. \tag{41}$$

According to (36), $H_{\text{p},\ell}$ can be expressed as

$$H_{\text{p},\ell} = \begin{cases} H_{t_{\text{SM}}}\left[\exp\left(-\frac{4\lambda_M V^2T^2(1-\lambda^*\xi)^2}{\pi\lambda^*\xi}\right) - \exp\left(-\frac{4\lambda_M V^2T_p^2(1-\lambda^*\xi_f)^2}{\pi\lambda^*\xi_f}\right)\right], & \ell = \text{SM} \\ H_{t_{S'S}}\left[Q_1\left(\frac{1}{2\sigma\sqrt{\lambda_S}}, \frac{2TV(1-\lambda^*\xi)}{\pi\sigma\sqrt{\lambda^*\xi}}\right) - Q_1\left(\frac{1}{2\sigma\sqrt{\lambda_S}}, \frac{2T_pV(1-\lambda^*\xi_f)}{\pi\sigma\sqrt{\lambda^*\xi_f}}\right)\right], & \ell = S'S \\ H_{t_{S'M}}\left[Q_1\left(\frac{1}{2\sigma\sqrt{\lambda_M}}, \frac{2TV(1-\lambda^*\xi)}{\pi\sigma\sqrt{\lambda^*\xi}}\right) - Q_1\left(\frac{1}{2\sigma\sqrt{\lambda_M}}, \frac{2T_pV(1-\lambda^*\xi_f)}{\pi\sigma\sqrt{\lambda^*\xi_f}}\right)\right], & \ell = S'M. \end{cases} \tag{42}$$

V. Numerical Results and Discussion

In this section, we verify the analytical results of the handover performance which have been derived in the above sections. In this article, we focus on the cross-tier handovers between the two tiers of SBSs. The cross-tier handovers

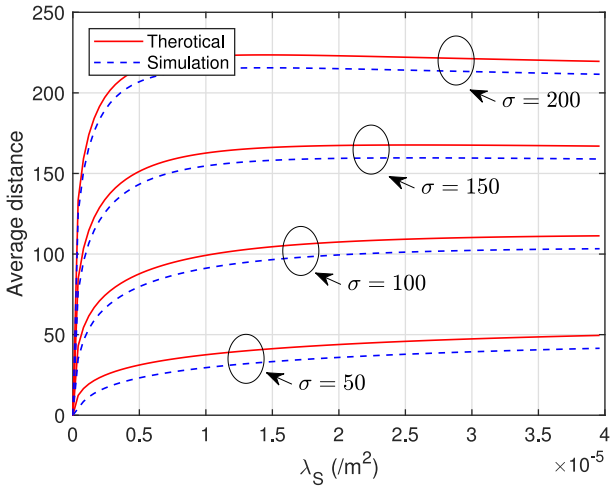

Fig. 5. Average distance from the PCP distributed SBSs to the PPP distributed SBSs as a function of SBS density λ_S.

between MBSs and SBSs following PPP distribution, and those handovers occur in the same MBSs and SBSs ties have been investigated in the previous papers [12], [13], [15], [16], [17]. The cross-tier handovers between MBSs and SBSs following PCP distribution share the same analytical method in our manuscript. As for the same tier, those handovers occur in the MBSs and SBSs following PPP with different densities share the same analytical method with [27]. The simulation area is set as a 5 km × 5 km square where three-tiers dense BSs are deployed. According to [28], the path loss of macro cells and small cells at distance r are $128.1+37.6\log_{10}(r)$ dB and $140.7+36.7\log_{10}(r)$ dB, respectively. The parameters of different cells are set as $P_M = 46$ dBm, $P_S = P_{S'} = 30$ dBm, $G_M = 14$ dBi, $G_S = G_{S'} = 5$ dBi, $B_M = 0$ dB, and $B_S = B_{S'} = 4$ dB. And Q_{out} is set as -8 dB according to [42]. For dense deployments, we assume $\lambda_S = 10\lambda_M = 10\lambda_p$.

Fig. 5 shows the average distance $R_{S'S}$ as a function of λ_S under different σ. As shown in Fig. 5, the average value of $R_{S'S}$ increases with λ_S at first, and then tends to a stable value which is affected by σ. It indicates that in the PCP HetNets, the average $R_{S'S}$ is mainly effected by σ and λ_S has only limited influence when σ is much larger than λ_S. This phenomenon is different from the results derived in PPP-based models. According to Section II-B, the nodes in the MRWP model tend to distribute in edge areas when the node density is small. Thus, the average $R_{S'S}$ will increase with λ_S at the beginning.

Fig. 6 shows the handover rate as a function of λ_S and σ under different thresholds T. From Fig. 6(a), we can see that the handover rate follows the same trend with the average value of $R_{S'S}$. The handover rate consists of the handover trigger rate and the probability that the handover UE's sojourn time inside the small cell is larger than the threshold T. Because the handover triggered rate is approximately proportional to $R_{S'S}$ and $R_{S'S}$ is mainly affected by σ, the corresponding radius of each ERB will remain as a stable value with the increase of λ_S when σ is a constant. When the UE moves into the ERB circle, the average transmission time is more likely to be smaller than a larger T, which is

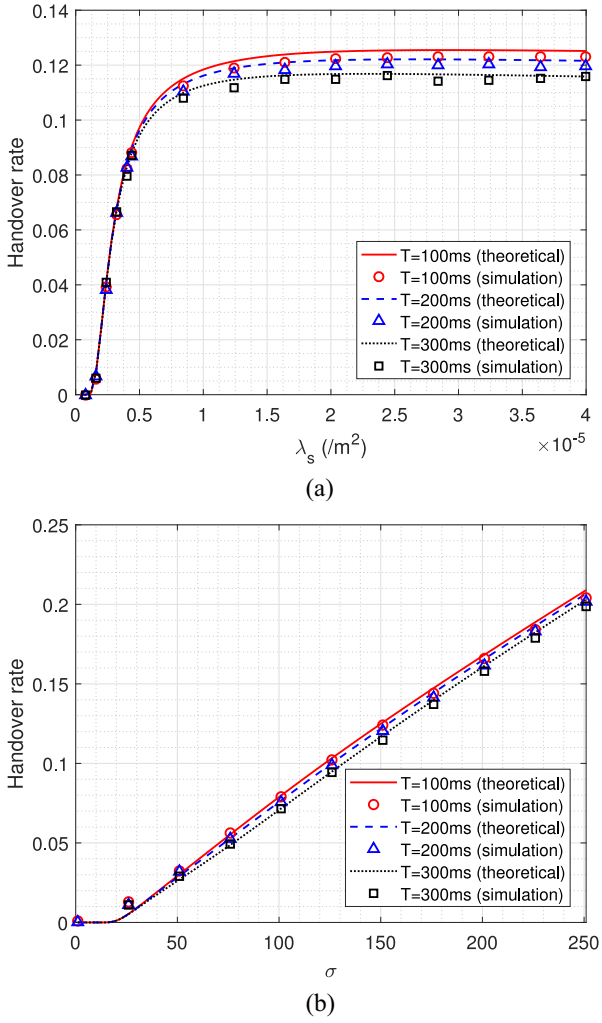

Fig. 6. Handover rate as a function of BS density and scattering standard variance at different sojourn time thresholds T when $P_{S'} = 30$ dBm and $V = 60$ km/h. (a) Impact of PPP distributed SBS density λ_S when $\sigma = 150$. (b) Impact of PCP distributed SBS standard variance σ when $\lambda_S = 2 \times 10^{-5}$/m^2.

obvious because the relative radius of the ERB is the function of $R_{S'S}$ and the average transmission time shares the same trend with $R_{S'S}$. The increasing threshold T will lead to a lower handover rate as shown in Fig. 6(a). In Fig. 6(b), the handover rate monotonically increases with σ. According to (10) and the results in Fig. 5, we conclude that the radius of ERB monotonically increases with average distance $R_{S'S}$. Since the average distance $R_{S'S}$ is proportional to σ, the radius of ERB will also rise with the increasing σ. In that case, the rising radius of ERB will result in higher coverage in each cluster. Since the sojourn time for the user rises in a larger coverage, $\mathbb{P}(S_{S'S} \geq T)$ grows with the increase of σ, thus leading to a higher handover rate.

The velocity of users will also influence the handover performance. As shown in Fig. 7(a), the handover rate rises with the increasing V, which is obvious since the handover triggered rate is proportional to V according to (34). When average distance $\bar{R}_\ell$ is unchanged, $\mathbb{P}(S_\ell \geq T)$ will decrease with the increasing V. However, the trend of the decrease is nonlinear. As we can see in Fig. 7(a), with the increasing V,

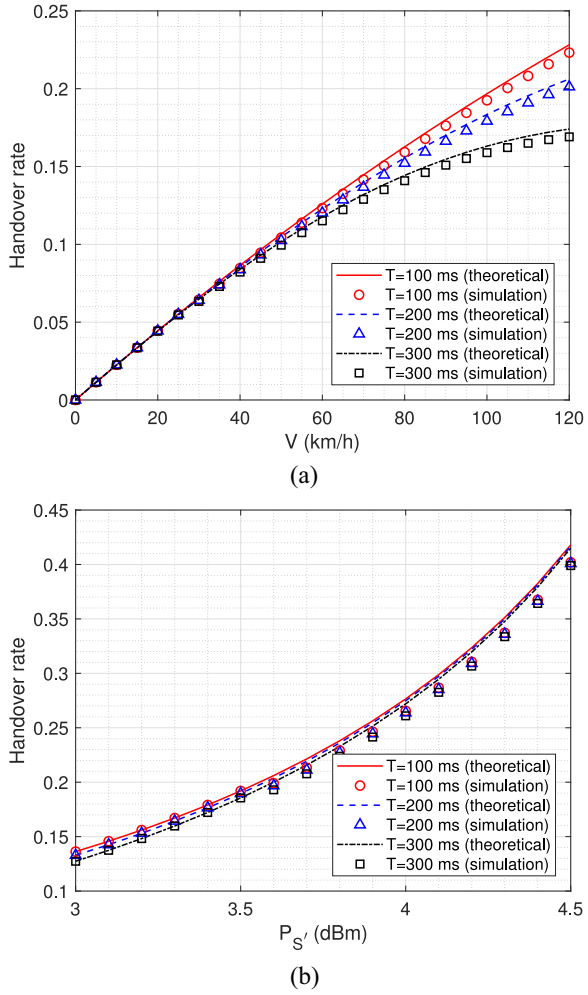

Fig. 7. Handover rate as a function of velocity V and transmit power $P_{S'}$ at different sojourn time thresholds T when $\lambda_S = 2 \times 10^{-5}/\text{m}^2$ and $\sigma = 150$. (a) Impact of velocity V when $P_{S'} = 30\,\text{dBm}$. (b) Impact of transmit power $P_{S'}$ when $V = 60\,\text{km/h}$.

the handover rate shows a trend from rising to declining gradually, which can be explained by the fact that $\mathbb{P}(S_\ell \geq T)$ has reached the nonlinear part. Fig. 7(b) presents how the transmit power of typical BS influences the handover performance. When the transmit power P_ℓ of target BS is assigned with a stable value, the handover rate rises with the increasing transmit power $P_{S'}$ of typical BS. As shown in Section III-A, the radius of ERB circle is determined by the ratio of $P_{S'}$ and P_ℓ. With the increasing $P_{S'}$, the radius of ERB circle will rise. From the simulations analysis, the higher $P_{S'}$ brings larger radius of ERB circle, which means the specific area in Section IV-A gets larger. With unchanged simulation region, the ratio of specific area and the whole coverage will rise since the handover trigger rate of one target BS in the entire area increases. Eventually, the handover rate rises with the increasing $P_{S'}$. It is a remarkable fact that the simulation result is lower than the theoretical analysis, which is mainly because the theoretical results are calculated by one movement for each user. While in simulation those users may have multiple trace movements inside one ERB circle, which could increase the sojourn time for the user. The other reason is that the average distance is set as the upper boundary when doing the calculation, therefore the upper boundary of theoretical curves will be higher than the simulation curves. Similar simulation results can be found in [20] and [27].

Fig. 8 illustrates the handover failure rate as a function of λ_S, V, $P_{S'}$, and σ under different thresholds T. As shown in Fig. 8(a), $H_{f,\ell}$ grows with the rising of λ_S and threshold T. Each of the curves increases at the early stage remarkably and then slowly down the growth. This result can be explained by the fact that the handover failure triggered rate $H_{f,t}$ shares the same trend with $R_{S'S}$, thus the handover failure rate under this condition is mainly determined by $\mathbb{P}(S_{f,S'S} \leq T)$. Since the Marcum Q-function decreases remarkably at the early stage and then converges to minimum, $\mathbb{P}(S_{f,S'S} \leq T)$ will follow the opposite trend with the Marcum Q-function according to (40). We can also see that the handover failure rate slowly reaches a stable value, which is determined by the ratio of $H_{f,t,S'S}$ and $H_{t,S'S}$. Note that H_f decreases with the decrease of T. This is because the distance between handover circle and handover failure circle $S_{f,\ell}$ rises with the decreasing Q_{out}. With smaller T, the users do not have enough time to reach the handover failure circle, thus the handover failure event cannot be initiated successfully. According to Fig. 8(b), H_f decreases with the increase of σ. The reason is that greater σ leads to larger radius of the ERB circle, thus increasing the length of trajectory between the ERBs of handover circle and handover failure circle that a UE needs to pass through when the range expansion biases are different. Eventually, the probability that a UE touches the handover failure boundary in a unit time will decrease, which leads to a lower handover failure rate.

Fig. 8(c) shows the trend that the handover failure rate under different threshold T rises with the increasing V. This trend can be explained by the fact that the handover failure triggered rate $H_{f,t,\ell}$ rises with the increasing V. In the meantime, the sojourn time $S_{f,\ell}$ for the typical UE between handover boundary and handover failure boundary will decrease because the average distance is unchanged and the velocity is rising, which bring to the fact $\mathbb{P}(S_{f,\ell} \leq T)$ will also rise with the increasing V.

From the simulation results in Fig. 8(d), we can see that the handover failure rate $H_{f,\ell}$ decreases with the increasing $P_{S'}$. Moreover, the influence of $P_{S'}$ on $H_{f,\ell}$ is different from H_ℓ. During the handover failure rate analysis, the handover failure triggered rate shares the same trend with handover triggered rate. They will both rise with the increasing $P_{S'}$. However, $\mathbb{P}(S_{f,\ell} \leq T)$ decreases with the increasing $P_{S'}$, because the average distance between two ERB circles gets larger with the increasing $P_{S'}$, thus $S_{f,\ell}$ will rise since the velocity of the user remains unchanged. If T remains a stable value, $\mathbb{P}(S_{f,\ell} \leq T)$ will decrease with the increasing $P_{S'}$. To be noticed, the decrease of the handover failure rate is nonlinear, because $\mathbb{P}(S_{f,\ell} \leq T)$ is a Marcum Q-function and the decrease of which is nonlinear as we described in Fig. 7.

As illustrated in Fig. 9(a), the ping-pong rate rises and remains a much small value with the increase of λ_S. According to Fig. 9(b), with the increase of σ, the ping-pong rate first rises at the early stage and then slowly decreases. It is worth noting that the ping-pong rate decreases after reaching the maximum value, which can be explained by the fact that with

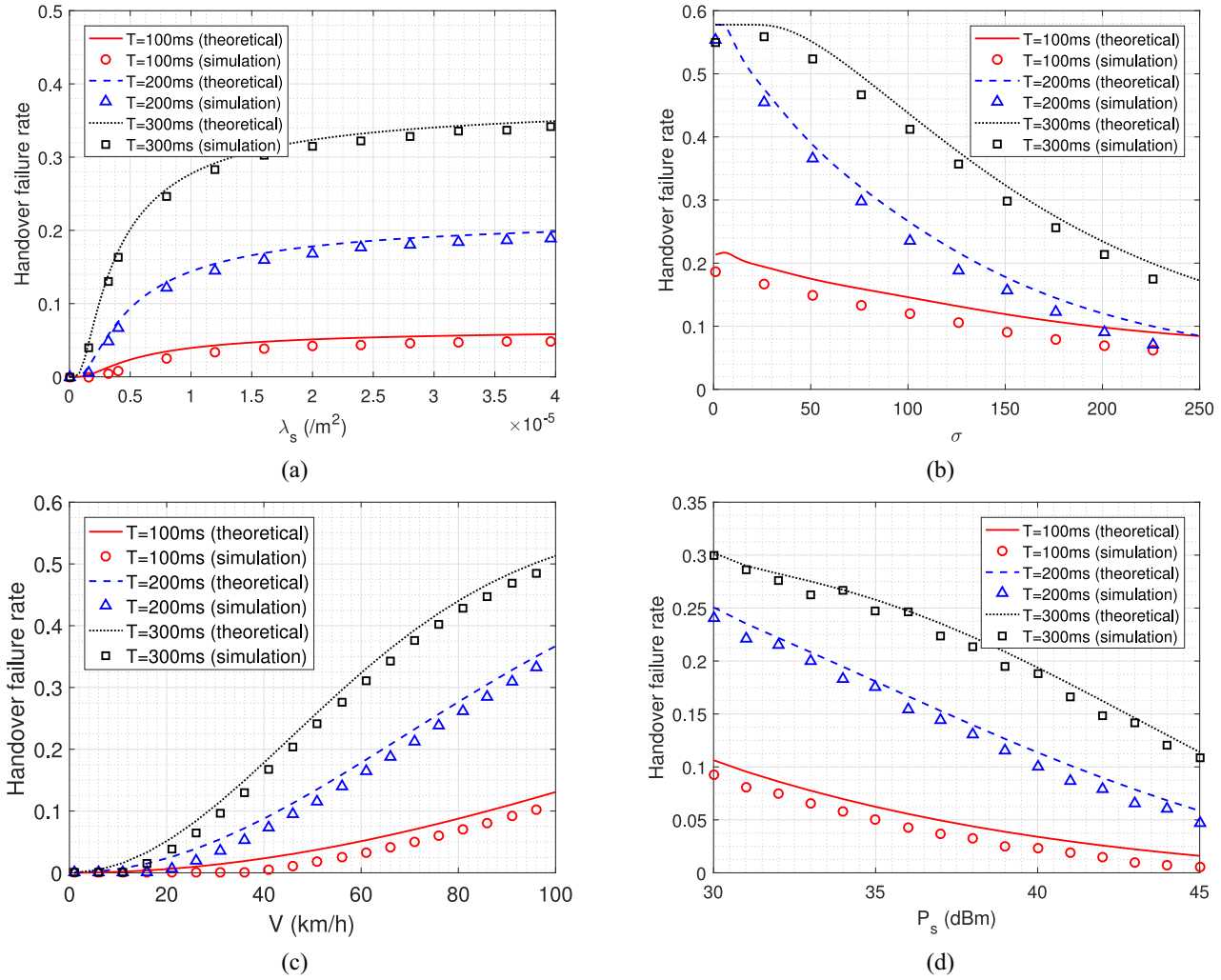

Fig. 8. Handover failure rate as a function of BS density, scattering standard variance, velocity, and transmit power at typical BS with different sojourn time thresholds. (a) Impact of λ_S when $\sigma = 150$. (b) Impact of σ when $\lambda_S = 2 \times 10^{-5}/\text{m}^2$. (c) Impact of V when $P_S = 30\,\text{dBm}$. (d) Impact of P_S when $V = 60\,\text{km/h}$.

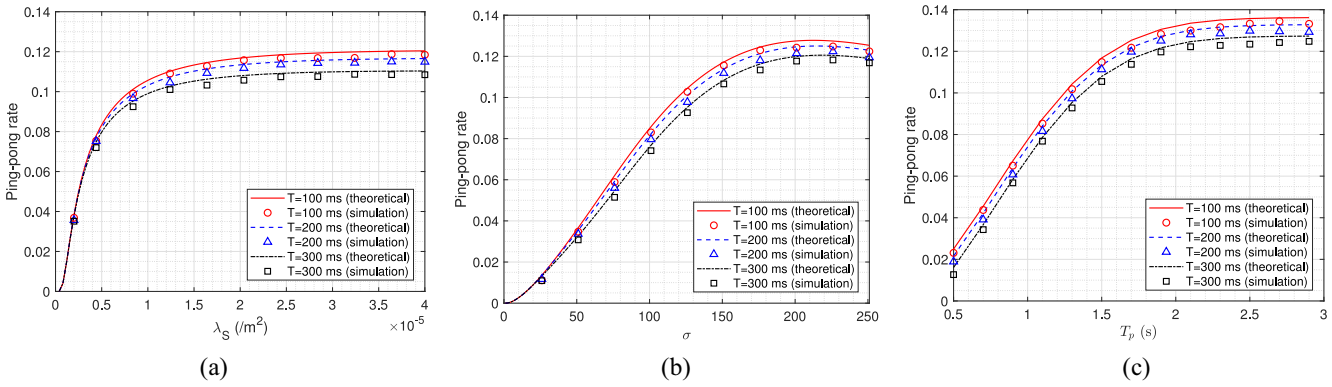

Fig. 9. Ping-pong rate as a function of BS density, scattering standard variance, and threshold T_p at different sojourn time thresholds. (a) Impact of λ_S when $\sigma = 150$ and $T_p = 1.5\,\text{s}$. (b) Impact of σ when $\lambda_S = 2 \times 10^{-5}/\text{m}^2$ and $T_p = 1.5\,\text{s}$. (c) Impact of T_p when $\lambda_S = 2 \times 10^{-5}/\text{m}^2$ and $\sigma = 150$.

the increase of σ, the average distance rises, so does the corresponding radius of ERB circle. The rising σ will increase the average distance. In that case the ping-pong rate will decrease because when the UE moves back, it may change the moving direction before it touches the original serving BS's boundary. The longer average distance means that the UE is more likely to move into other cells. However, the rising σ will also increase the corresponding radius of the ERB circle. For the ping-pong rate, the bigger radius indicates the larger cell area, which will increase the probability that the UE touches

the original boundary when it comes back. As illustrated in Fig. 9(c), the ping-pong rate rises with the increase of T_p and saturates to a stable value. It is obvious that larger T_p will increase the time consumed by the handover decision.

VI. Conclusion

In order to derive the handover performance in HetNets under PCP scenarios, we have proposed an MRWP model to improve simulation accuracy by eliminating the DWP. Then, we finished the analysis of the BSs locations distribution under PPP and PCP. Based on the analytical model, we have derived the theoretical expressions of different handover metrics, including handover rate, handover failure rate, and ping-pong rate under PCP distribution scenarios, which is the first time in the recent literature. The accuracy of the proposed model and methods is validated through Monte Carlo simulations. As illustrated in Section V, those expressions are determined by deployment intensity, scattering variance of TCP, the threshold of triggered time, and velocity. The results reveal that applying the MRWP model in traffic hotspots can lead to better coverage performance in edge area than the traditional RWP model. Moreover, compared with the BS density, the scattering variance of small cells has more significant impact on the average distance and handover rate. The threshold T should set as a small value, since smaller T can significantly decreases the handover failure rate while slightly rises the handover rate and ping-pong rate. To get a balanced handover performance, σ should be carefully selected to tradeoff the handover rate, handover failure rate, and the ping-pong rate. Those findings in user-centric area and high-density deployments networks can provide guidance for researchers to study the handover performance in ultradense areas. For instance, the vast amounts of users' handover analysis in 5G/6G networks where multi-BSs are deployed in one small traffic hotspots. In future work, we intend to investigate the multiobjectives optimization problems between those critical parameters to get better performance in different actual applications.

Appendix A
Proof of Lemma 1

Let $q = \sqrt{x_j^2 + y_j^2}$ and $F(\lambda) = \int_0^q E(r)\,dr$. Recalling (8), $F(\lambda)$ can be formulated by

$$F(\lambda) = \int_0^q \left| r^{2\alpha_{ij}} - \lambda r^2 \right| dr. \tag{43}$$

Taking the derivative of $F(\lambda)$ with respect to λ yields $F'(\lambda) = -(q^3/3) + (1/3)\lambda^{[3/2(\alpha-1)]}$, $\lambda \le r^{2(\alpha-1)}$. Then, $F'(\lambda) = 0$ yields $\lambda = q^{2(\alpha-1)}$. When $\lambda > r^{2(\alpha-1)}$, there is no minimum value of $F(\lambda)$.

Appendix B
Proof of Theorem 1

Assume the typical BS located at the origin and the hotspot center at $\|\mathbf{x}_0\| = (x_0, y_0) \in \Phi_p$. Since the offspring SBSs $B_{\mathbf{x}_0}$ generated from $\|\mathbf{x}_0\|$ following symmetric normal distribution with variance σ^2, the coordinate of $X \in B_{\mathbf{x}_0}$ can be determined by the PDF as follows:

$$f_{R_{S'S}|W_S}(x, y \mid \|\mathbf{x}_0\|) = \frac{1}{2\pi\sigma^2} \exp\left\{ -\frac{(x-x_0)^2 + (y-y_0)^2}{2\sigma^2} \right\}. \tag{44}$$

The CDF of $R_{S'S} \triangleq \sqrt{x^2 + y^2}$ is then formulated by

$$\begin{aligned} F_{R_{S'S}|W_S}(r|\|\mathbf{x}_0\|) &= \int_{\mathcal{B}(O,r)} f_{R_{S'S}}(x, y|\|\mathbf{x}_0\|)dxdy \\ &\overset{(a)}{=} \int_0^r \int_0^{2\pi} r f_{R_{S'S}}(r\cos\theta, r\sin\theta|\|\mathbf{x}_0\|)d\theta dr \\ &= \int_0^r \frac{r}{2\pi\sigma^2} \exp\left\{ -\frac{r^2 + x_0^2 + y_0^2}{2\sigma^2} \right\} \\ &\quad \times \int_0^{2\pi} \exp\left\{ \frac{r(x_0\cos\theta + y_0\sin\theta)}{\sigma^2} \right\} d\theta dr \end{aligned} \tag{45}$$

where (a) follows by converting Cartesian into polar coordinates, i.e., $(x, y) \to (r\cos\theta, r\sin\theta)$. Then taking the derivative of $F_{R_{S'S}}(r|\|\mathbf{x}_0\|)$ with respect to r yields

$$\begin{aligned} f_{R_{S'S}|W_S}(r|\|\mathbf{x}_0\|) &= \frac{r}{2\pi\sigma^2} \exp\left(-\frac{r^2 + x_0^2 + y_0^2}{2\sigma^2} \right) \\ &\quad \times \int_0^{2\pi} \exp\left\{ \frac{r(x_0\cos\theta + y_0\sin\theta)}{\sigma^2} \right\} d\theta. \end{aligned} \tag{46}$$

Let $w_0 = \sqrt{x_0^2 + y_0^2}$, we further have

$$\begin{aligned} f_{R_{S'S}|W_S}(r|w_0) &= \frac{r}{2\pi\sigma^2} e^{-\frac{r^2+w_0^2}{2\sigma^2}} \int_0^{2\pi} \exp\left\{ \frac{r(x_0\cos\theta + y_0\sin\theta)}{\sigma^2} \right\} d\theta \\ &\overset{(a)}{=} \frac{r}{\pi\sigma^2} \exp\left(-\frac{r^2 + w_0^2}{2\sigma^2} \right) \int_0^{\pi} \exp\left(\frac{r w_0 \cos\theta}{\sigma^2} \right) d\theta \end{aligned} \tag{47}$$

where (a) follows from the periodicity of the trigonometric function and the symmetry of the cosine function. Finally, leveraging the definition of the modified Bessel function of the first kind completes the proof.

References

[1] R. Arshad, H. ElSawy, S. Sorour, T. Y. Al-Naffouri, and M. Alouini, "Handover management in dense cellular networks: A stochastic geometry approach," in *Proc. IEEE ICC*, Jun. 2015, pp. 3429–3434.

[2] X. Yang, X. Wang, Y. Wu, L. P. Qian, W. Lu, and H. Zhou, "Small-cell assisted secure traffic offloading for Narrowband Internet of Thing (NB-IoT) systems," *IEEE Internet Things J.*, vol. 5, no. 3, pp. 1516–1526, Jun. 2018.

[3] A. Damnjanovic et al., "A survey on 3GPP heterogeneous networks," *IEEE Wireless Commun.*, vol. 18, no. 3, pp. 10–21, Jun. 2011.

[4] Z. Ni, J. A. Zhang, X. Huang, K. Yang, and J. Yuan, "Uplink sensing in perceptive mobile networks with asynchronous transceivers," *IEEE Trans. Signal Process.*, vol. 69, pp. 1287–1300, Feb. 2021.

[5] X. Gao, D. Niyato, K. Yang, and J. An, "Cooperative scheme for backscatter-aided passive relay communications in wireless-powered D2D networks," *IEEE Internet Things J.*, vol. 9, no. 1, pp. 152–164, Jan. 2022.

[6] N. K. Panigrahy and S. C. Ghosh, "Analyzing the effect of soft handover on handover performance evaluation metrics under load condition," *IEEE Trans. Veh. Technol.*, vol. 67, no. 4, pp. 3612–3624, Apr. 2018.

[7] L. Ge, G. Chen, Y. Zhang, J. Tang, J. Wang, and J. A. Chambers, "Performance analysis for multihop cognitive radio networks with energy harvesting by using stochastic geometry," *IEEE Internet Things J.*, vol. 7, no. 2, pp. 1154–1163, Feb. 2020.
[8] J. G. Andrews, A. K. Gupta, and H. S. Dhillon, "A primer on cellular network analysis using stochastic geometry," 2016, *arXiv:1604.03183*.
[9] M. Afshang, C. Saha, and H. S. Dhillon, "Equi-coverage contours in cellular networks," *IEEE Wireless Commun. Lett.*, vol. 7, no. 5, pp. 700–703, Oct. 2018.
[10] C. Saha, H. S. Dhillon, N. Miyoshi, and J. G. Andrews, "Unified analysis of HetNets using Poisson cluster processes under max-power association," *IEEE Trans. Wireless Commun.*, vol. 18, no. 8, pp. 3797–3812, Aug. 2019.
[11] D. Lopez-Perez, I. Guvenc, and X. Chu, "Mobility management challenges in 3GPP heterogeneous networks," *IEEE Commun. Mag.*, vol. 50, no. 12, pp. 70–78, Dec. 2012.
[12] Y. Bi, G. Han, C. Lin, M. Guizani, and X. Wang, "Mobility management for intro/inter domain handover in software-defined networks," *IEEE J. Sel. Areas Commun.*, vol. 37, no. 8, pp. 1739–1754, Aug. 2019.
[13] A. Stamou, N. Dimitriou, K. Kontovasilis, and S. Papavassiliou, "Autonomic handover management for heterogeneous networks in a future Internet context: A survey," *IEEE Commun. Surveys Tuts.*, vol. 21, no. 4, pp. 3274–3297, 4th Quart., 2019.
[14] H. Yuan, N. Yang, K. Yang, C. Han, and J. An, "Hybrid beamforming for Terahertz multi-carrier systems over frequency selective fading," *IEEE Trans. Wireless Commun.*, vol. 68, no. 10, pp. 6186–6199, Oct. 2020.
[15] W. Bao and B. Liang, "Handoff rate analysis in heterogeneous wireless networks with Poisson and Poisson cluster patterns," in *Proc. 16th ACM Int. Symp. Mobile Ad Hoc Netw. Comput.*, Jun. 2015, pp. 77–86.
[16] W. Bao and B. Liang, "Stochastic geometric analysis of user mobility in heterogeneous wireless networks," *IEEE J. Sel. Areas Commun.*, vol. 33, no. 10, pp. 2212–2225, Oct. 2015.
[17] M. Shi, K. Yang, Z. Han, and D. Niyato, "Coverage analysis of integrated sub-6GHz-mmWave cellular networks with hotspots," *IEEE Trans. Wireless Commun.*, vol. 67, no. 11, pp. 8151–8164, Nov. 2019.
[18] M. Shi, X. Gao, K. Yang, D. Niyato, and Z. Han, "Meta distribution of the SINR for mmWave cellular networks with clusters," *IEEE Trans. Wireless Commun.*, vol. 69, no. 10, pp. 6956–6970, Oct. 2021.
[19] R. Arshad, H. Elsawy, L. Lampe, and M. J. Hossain, "Handover rate characterization in 3D ultra-dense heterogeneous networks," *IEEE Trans. Veh. Technol.*, vol. 68, no. 10, pp. 10340–10345, Oct. 2019.
[20] Y. Teng, A. Liu, and V. K. N. Lau, "Stochastic geometry based handover probability analysis in dense cellular networks," in *Proc. Int. Conf. Wireless Commun. Signal Process. (WCSP)*, Oct. 2018, pp. 1–7.
[21] R. Arshad, H. ElSawy, S. Sorour, T. Y. Al-Naffouri, and M.-S. Alouini, "Cooperative handover management in dense cellular networks," in *Proc. IEEE Globecom*, Dec. 2016, pp. 1–6.
[22] R. Arshad, H. ElSawy, S. Sorour, T. Y. Al-Naffouri, and M.-S. Alouini, "Velocity-aware handover management in two-tier cellular networks," *IEEE Trans. Wireless Commun.*, vol. 16, no. 3, pp. 1851–1867, Mar. 2017.
[23] H. Ibrahim, H. ElSawy, U. T. Nguyen, and M.-S. Alouini, "Mobility-aware modeling and analysis of dense cellular networks with *C*-plane/*U*-plane split architecture," *IEEE Trans. Commun.*, vol. 64, no. 11, pp. 4879–4894, Nov. 2016.
[24] B. Fang and W. Zhou, "Handover reduction via joint bandwidth allocation and CAC in randomly distributed HCNs," *IEEE Commun. Lett.*, vol. 19, no. 7, pp. 1209–1212, Jul. 2015.
[25] L. P. Qian, Y. Wu, H. Zhou, and X. Shen, "Dynamic cell association for non-orthogonal multiple-access V2S networks," *IEEE J. Sel. Areas Commun.*, vol. 35, no. 10, pp. 2342–2356, Oct. 2017.
[26] L. P. Qian, Y. Wu, H. Zhou, and X. Shen, "Non-orthogonal multiple access vehicular small cell networks: Architecture and solution," *IEEE Netw.*, vol. 31, no. 4, pp. 15–21, Jul. 2017.
[27] X. Xu, Z. Sun, X. Dai, T. Svensson, and X. Tao, "Modeling and analyzing the cross-tier handover in heterogeneous networks," *IEEE Trans. Wireless Commun.*, vol. 16, no. 12, pp. 7859–7869, Dec. 2017.
[28] "E-UTRA; further advancements for E-UTRA physical layer aspects," 3GPP, Sophia Antipolis, France, Rep. TR 36.814 V.11.1.0, Jan. 2013.
[29] C. Saha, M. Afshang, and H. S. Dhillon, "3GPP-inspired HetNet model using Poisson cluster process: Sum-product functionals and downlink coverage," *IEEE Trans. Commun.*, vol. 66, no. 5, pp. 2219–2234, May 2018.
[30] M. Afshang, H. S. Dhillon, and P. H. J. Chong, "Modeling and performance analysis of clustered device-to-device networks," *IEEE Trans. Wireless Commun.*, vol. 15, no. 7, pp. 4957–4972, Jul. 2016.
[31] C. Saha, M. Afshang, and H. S. Dhillon, "Enriched *K*-tier HetNet model to enable the analysis of user-centric small cell deployments," *IEEE Trans. Wireless Commun.*, vol. 16, no. 3, pp. 1593–1608, Mar. 2017.
[32] M. Afshang and H. S. Dhillon, "Poisson cluster process based analysis of HetNets with correlated user and base station locations," *IEEE Trans. Wireless Commun.*, vol. 17, no. 4, pp. 2417–2431, Apr. 2018.
[33] H. ElSawy, A. Sultan-Salem, M.-S. Alouini, and M. Z. Win, "Modeling and analysis of cellular networks using stochastic geometry: A tutorial," *IEEE Commun. Surveys Tuts.*, vol. 19, no. 1, pp. 167–203, 1st Quart., 2017.
[34] R. Zhang, M. Wang, X. Shen, and L. Xie, "Probabilistic analysis on QoS provisioning for Internet of Things in LTE-A heterogeneous networks with partial spectrum usage," *IEEE Internet Things J.*, vol. 3, no. 3, pp. 354–365, Jun. 2016.
[35] Y. Aydin, G. K. Kurt, E. Ozdemir, and H. Yanikomeroglu, "Group handover for drone-mounted base stations," *IEEE Internet Things J.*, vol. 8, no. 18, pp. 13876–13887, Sep. 2021, doi: 10.1109/JIOT.2021.3068297.
[36] D. B. Johnson and D. A. Maltz, "Dynamic source routing in ad hoc wireless networks," in *Mobile Computing*. Boston, MA, USA: Springer, 1996.
[37] X. Lin, R. K. Ganti, P. J. Fleming, and J. G. Andrews, "Towards understanding the fundamentals of mobility in cellular networks," *IEEE Trans. Wireless Commun.*, vol. 12, no. 4, pp. 1686–1698, Apr. 2013.
[38] C. Bettstetter, H. Hartenstein, and X. Pérez-Costa, "Stochastic properties of the random waypoint mobility model," *ACM/Kluwer Wireless Netw.*, vol. 10, no. 5, pp. 555–567, Sep. 2004.
[39] J. Kerdsri, "Visualization of spatial distribution of random waypoint mobility models," *J. Comput.*, vol. 12, no. 4, pp. 309–316, Jan. 2017.
[40] R. Salahat, E. Salahat, A. Hakam, and T. Assaf, "A simple and efficient approximation to the modified bessel functions and its applications to Rician fading," in *Proc. IEEE GCC Conf. Exhibition (GCC)*, Nov. 2013, pp. 351–354.
[41] D. López-Pérez, X. Chu, and İ. Guvenc, "On the expanded region of picocells in heterogeneous networks," *IEEE J. Sel. Topics Signal Process.*, vol. 6, no. 3, pp. 281–294, Jun. 2012.
[42] "Study on small cell enhancements for E-UTRA and E-UTRAN; higher layer aspects," 3GPP, Sophia Antipolis, France, Rep. TR 36.842 V.12.0.0, Dec. 2013.
[43] I. S. Gradshteyn and I. M. Ryzhik, *Table of Integrals, Series, and Products*. New York, NY, USA: Academic, 2014.
[44] R. Arshad, H. Elsawy, L. Lampe, and M. J. Hossain, "Handover rate characterization in 3D ultra-dense heterogeneous networks," *IEEE Trans. Veh. Technol.*, vol. 68, no. 10, pp. 10340–10345, Oct. 2019.

He Zhou received the B.E. and M.S. degrees from Harbin Institute of Technology, Harbin, China, in 2016 and 2018, respectively. He is currently pursuing the Ph.D. degree with the School of Information and Electronics, Beijing Institute of Technology, Beijing, China.

His research interests mainly include mobility management, satellite communication, matching theory, and space–air–ground integrated networks.

Haibo Zhou (Senior Member, IEEE) received the Ph.D. degree in information and communication engineering from Shanghai Jiao Tong University, Shanghai, China, in 2014.

From 2014 to 2017, he was a Postdoctoral Fellow with the Broadband Communications Research Group, Department of Electrical and Computer Engineering, University of Waterloo, Waterloo, ON, Canada. He is currently a Full Professor with the School of Electronic Science and Engineering, Nanjing University, Nanjing, China. His research interests include resource management and protocol design in B5G/6G networks, vehicular ad hoc networks, and space–air–ground integrated networks.

Prof. Zhou was a recipient of the 2019 IEEE ComSoc Asia–Pacific Outstanding Young Researcher Award. He served as the Track/Symposium Co-Chair for IEEE/CIC ICCC 2019, IEEE VTC-Fall 2020, IEEE VTC-Fall 2021, and IEEE GLOBECOM 2022. He is currently an Associate Editor of the IEEE TRANSACTIONS ON WIRELESS COMMUNICATIONS, IEEE INTERNET OF THINGS JOURNAL, *IEEE Network Magazine*, and IEEE WIRELESS COMMUNICATIONS LETTERS.

Jianguo Li received the B.E. and Ph.D. degrees from Beijing Institute of Technology, Beijing, China, in 2015 and 2022, respectively.

He is currently an Assistant Professor with the School of Cyberspace Science and Technology, Beijing Institute of Technology. His research interests include millimeter-wave communication, high-precision radar, and high data rate modulation and demodulation.

Kai Yang (Member, IEEE) received the B.E. degree in communications engineering from the National University of Defense Technology, Changsha, China, in 2005, and the Ph.D. degree in communications engineering from Beijing Institute of Technology, Beijing, China, in 2010.

From January 2010 to July 2010, he was with the Department of Electronic and Information Engineering, Hong Kong Polytechnic University, Hong Kong. From 2010 to 2013, he was with Alcatel-Lucent Shanghai Bell, Shanghai, China. In 2013, he joined the Laboratoire de Recherche en Informatique, University Paris Sud 11, Orsay, France. He is currently with the School of Information and Electronics, Beijing Institute of Technology. His current research interests include convex optimization, massive MIMO, mmWave systems, resource allocation, and interference mitigation.

Jianping An (Senior Member, IEEE) received the Ph.D. degree from Beijing Institute of Technology, Beijing, China, in 1996.

He joined the School of Information and Electronics, Beijing Institute of Technology in 1996, where he is currently a Full Professor and the Dean of the School of Cyberspace Science and Technology. His research interests are in the field of digital signal processing, cognitive radio, wireless networks, and high-dynamic broadband wireless transmission technology.

Xuemin (Sherman) Shen (Fellow, IEEE) received the Ph.D. degree in electrical engineering from Rutgers University, New Brunswick, NJ, USA, in 1990.

He is a University Professor with the Department of Electrical and Computer Engineering, University of Waterloo, Waterloo, ON, Canada. His research focuses on network resource management, wireless network security, Internet of Things, 5G and beyond, and vehicular ad hoc and sensor networks.

Dr. Shen received the Canadian Award for Telecommunications Research from the Canadian Society of Information Theory in 2021, the R. A. Fessenden Award in 2019 from IEEE, Canada, the Award of Merit from the Federation of Chinese Canadian Professionals (Ontario) in 2019, the James Evans Avant Garde Award in 2018 from the IEEE Vehicular Technology Society, the Joseph LoCicero Award in 2015 and the Education Award in 2017 from the IEEE Communications Society, and the Technical Recognition Award from Wireless Communications Technical Committee in 2019 and AHSN Technical Committee in 2013. He has also received the Excellent Graduate Supervision Award in 2006 from the University of Waterloo and the Premiers Research Excellence Award in 2003 from the Province of Ontario, Canada. He served as the Technical Program Committee Chair/Co-Chair for IEEE Globecom 16, IEEE Infocom14, IEEE VTC10 Fall, and IEEE Globecom07, and the Chair for the IEEE Communications Society Technical Committee on Wireless Communications. He is the President of the IEEE Communications Society. He was the Vice President for Technical and Educational Activities, the Vice President for Publications, a Member-at-Large on the Board of Governors, the Chair of the Distinguished Lecturer Selection Committee, and a member of IEEE Fellow Selection Committee of the ComSoc. He served as the Editor-in-Chief for the IEEE INTERNET OF THINGS JOURNAL, IEEE NETWORK, and *IET Communications*. He is a registered Professional Engineer of Ontario, Canada, an Engineering Institute of Canada Fellow, a Canadian Academy of Engineering Fellow, a Royal Society of Canada Fellow, a Chinese Academy of Engineering Foreign Member, and a Distinguished Lecturer of the IEEE Vehicular Technology Society and Communications Society.